NUREG/CR-2774 Vol. I
ANL-82-24 Vol. I

NUREG/CR-2774 Vol. I
ANL-82-24 Vol. I

PHYSICS OF REACTOR SAFETY

Quarterly Report
January—March 1982

ARGONNE NATIONAL LABORATORY

ARGONNE NATIONAL LABORATORY, ARGONNE, ILLINOIS

Prepared for the Office of Nuclear Regulatory Research
U. S. NUCLEAR REGULATORY COMMISSION
under Interagency Agreement DOE 40-550-75

The facilities of Argonne National Laboratory are owned by the United States Government. Under the terms of a contract (W-31-109-Eng-38) among the U. S. Department of Energy, Argonne Universities Association and The University of Chicago, the University employs the staff and operates the Laboratory in accordance with policies and programs formulated, approved and reviewed by the Association.

MEMBERS OF ARGONNE UNIVERSITIES ASSOCIATION

The University of Arizona
Carnegie-Mellon University
Case Western Reserve University
The University of Chicago
University of Cincinnati
Illinois Institute of Technology
University of Illinois
Indiana University
The University of Iowa
Iowa State University
The University of Kansas
Kansas State University
Loyola University of Chicago
Marquette University
The University of Michigan
Michigan State University
University of Minnesota
University of Missouri
Northwestern University
University of Notre Dame
The Ohio State University
Ohio University
The Pennsylvania State University
Purdue University
Saint Louis University
Southern Illinois University
The University of Texas at Austin
Washington University
Wayne State University
The University of Wisconsin-Madison

Available from

GPO Sales Program
Division of Technical Information and Document Control
U. S. Nuclear Regulatory Commission
Washington, D.C. 20555

and

National Technical Information Service
Springfield, Virginia 22161

NUREG/CR-2774 Vol. I
ANL-82-24 Vol. I

(Distribution
Code: R7)

ARGONNE NATIONAL LABORATORY
9700 South Cass Avenue
Argonne, Illinois 60439

PHYSICS OF REACTOR SAFETY

Quarterly Report
January—March 1982

Applied Physics Division
Components Technology Division

May 1982

Previous reports in this series

ANL-81-29 (I)	January—March 1981
ANL-81-29 (II)	April—June 1981
ANL-81-29 (III)	July—September 1981
ANL-81-29 (IV)	October—December 1981

Prepared for the Division of Reactor Safety Research
Office of Nuclear Regulatory Research
U. S. Nuclear Regulatory Commission
Washington, D. C. 20555
Under Interagency Agreement DOE 40-550-75

NRC FIN Nos. A2015 and A2045

PHYSICS OF REACTOR SAFETY

Quarterly Report
January-March 1982

ABSTRACT

This Quarterly progress report summarizes work done during the months of January-March 1982 in Argonne National Laboratory's Applied Physics and Components Technology Divisions for the Division of Reactor Safety Research of the U.S. Nuclear Regulatory Commission. The work in the Applied Physics Division includes reports on reactor safety modeling and assessment by members of the Reactor Safety Appraisals Section. Work on reactor core thermal-hydraulics is performed in ANL's Components Technology Division, emphasizing 3-dimensional code development for LMFBR accidents under natural convection conditions. An executive summary is provided including a statement of the findings and recommendations of the report.

FIN No.	Title
A2015	Reactor Safety Modeling and Assessment
A2045	3-D Time-dependent Code Development

TABLE OF CONTENTS

LIST OF FIGURES

LIST OF TABLES

EXECUTIVE SUMMARY

The BIFLO code has been modified to simplify the input required for non-hexagonal bundle geometries and to allow all channels to exchange energy with a portion of the bundle wall.

Calculations of a 15-pin sodium boiling experiment in the OPERA Facility have been completed using BIFLO in response to the experimenters' request for code developers to participate in a pretest calculational exercise. BIFLO calculations were performed using both one- and two-dimensional geometries. Inlet flow reversal was calculated to occur ~0.55 s after boiling developed across the entire bundle flow area regardless of the geometry being used; however, the timing of inlet flow reversal relative to the beginning of the flow coastdown was calculated to be ~0.9 s earlier using a two-dimensional geometry than was calculated using a one-dimensional geometry. The experiment was performed after the calculations were completed, but the experimental results have not been released.

A number of preliminary LOF and TOP calculations have been completed for the CRBR heterogeneous core in support of licensing proceedings, using the SAS/EPIC code. Points in the fuel cycle considered were BOC-1, EOC-3, and EOC-4. For the TOP calculations effort has been concentrated so far on the EOC-3 state, because the large number of driver subassemblies operating at about the same power produces a tendency for autocatalysis when fuel motion feedback is positive. This tendency became evident when fuel pin failure was assumed to be at the core midplane, as suggested by the W2 SLSF experiment. A number of parametric variations were made; the most important were found to be the assumed positive reactivity ramp rate and the rate of fuel sweepout in the coolant channel. For a ramp rate of 4 ¢/sec, credible for an uncontrolled rod withdrawal, no problem was encountered. For 10 ¢/sec and higher, however, autocatalytic tendencies appeared, producing hydrodynamic disassembly conditions.

The LOF calculations have so far been performed only for EOC-4. Clad motion effects were small because of the use of the CMOT code. It was found that there was some tendency for LOF-TOP development even in this low sodium void worth core if there was positive fuel motion feedback corresponding to gravity acceleration in excess of 0.1 g.

In the case of COMMIX-1A development work, several improvements and modifications have been implemented. Most of the improvements are in the area of dynamic storage, thermal structure model, and graphic package. Efforts have begun to document and release the code.

In the area of validation of COMMIX for preparation of CRBR licensing, three simulations (FFTF, EBR-II, and CRBR) are being performed. The FFTF and EBR-II simulations are near completion and reports are under preparation. The results of steady-state simulation of FFTF are presented in technical report NUREG/CR-2535. The simulation of CRBR primary vessel has been initiated.

In the area of COMMIX-2 development work, most efforts were devoted to parametric studies and to resimulation of the German seven-pin transient test.

In the area of BODYFIT code development, a new pressure scheme has been implemented. This new scheme appears to have speeded up the rate of convergence significantly. This new scheme will now be tested in the calculation of flows in a 90°-bend elbow.

I. REACTOR SAFETY MODELING AND ASSESSMENT

(A2015)

A. BIFLO Code Development (P. L. Garner)

1. Modeling Changes

The coding in BIFLO has been modified in two areas: input and wall modeling. The subroutine which processes the input has been modified to simplify the specification of a geometry which is not a full hexagonal bundle. Although nonhexagonal geometries could be specified in the previous version, the input preparation was rather cumbersome. The modeling in BIFLO has been extended to allow all flow channels to exchange energy with a portion of the bundle wall; the previous BIFLO formulation allowed only the highest numbered channel to exchange energy with the bundle wall. These modifications were needed to facilitate analysis of the 15-pin triangular bundle geometry of an OPERA Facility experiment.

2. Pretest Calculations of 15-Pin OPERA Experiment Using BIFLO

Pretest calculations have been performed for a loss-of-flow experiment which was subsequently performed in a 15-pin bundle in the OPERA Facility at ANL. These calculations were performed in response to a request from the experimenters for various groups actively involved in modeling sodium boiling to participate in a pretest analysis. Various groups submitted calculations using SAS4A, LIMBO, BIFLO, and SABRE (and possibly other codes) before the experiment was performed in March 1982. A compilation of the pretest calculations and the detailed experimental results will be released in the future by the experimenters.

The triangular geometry of the 15-pin bundle is representative of somewhat more than a one-sixth sector of a 61-pin hexagonal bundle; this geometry provides a better representation of the radial temperature distribution in a full-size 217-pin bundle than has been possible in earlier 1- and 7-pin OPERA experiments. The pin diameter, pin-to-pin spacing, heated length, and plenum length are identical to those dimensions for a FFTF fuel assembly. The pins are electrically heated internally; the power generation is uniform, both axially within a pin and from pin-to-pin. For reference in the following discussion, Pins 1, 11, and 15 are located at the three corners of the bundle, and Pin 1 corresponds to the center pin of a 61-pin hexagonal bundle. The thermal and hydraulic effects of two of the bundle walls (from Pin 1 to Pin 11 and from Pin 1 to Pin 15) have been minimized by placing filler wires on these walls and small-diameter wire wraps on the pins adjacent to these walls. The third wall (which runs from Pin 11 to Pin 15 and simulates the wall of a hexagonal bundle) does not have filler wires; pins adjacent to this wall (except Pins 11 and 15) and all pins in the bundle interior have full-diameter wire wraps. Sodium flows from a pressurized supply tank, up through the test bundle, to a receiver tank in a once-through manner. The flow coastdown is shaped (by varying the supply tank pressure as a function of time) to simulate that calculated for a loss-of-flow scenario in FFTF. Further details of the geometry and conditions of the experiment are given in Reference 1.

One- and two-dimensional BIFLO calculations of this experiment have been performed based on the information contained in the pretest report.[1] The two-dimensional calculations utilized 4 channels, grouping together regions of the bundle having similar power-to-flow ratios and attempting to preserve the important aspects of the detailed coolant temperature distribution: the sodium adjacent to the side of the triangle which simulates the hexcan wall (i.e. from Pin 11 to Pin 15) is the coldest, and the opposite corner of the bundle (i.e. adjacent to Pin 1) is the hottest. Several different arrangements of the 4 channels were actually used in order to investigate the effects of the hot region expected in the bundle corner adjacent to Pin 1. The temperature rise in this corner has the potential to be 50 to 100% larger than the bundle-average temperature rise. Calculational geometries which treated this corner region as a single channel showed an earlier boiling initiation time but a similar overall voiding progression when compared with calculations performed in geometries which lumped this corner region with other portions of the bundle.

The computational mesh system used in BIFLO modeled only the pin bundle region. The axial flow equations in BIFLO use pressure as the boundary condition at the bottom and top of the computational mesh system. Consequently, the pressure histories shown in Reference 1 for the supply and receiver tanks were modified to account for the piping losses and elevation changes in order to obtain the bundle inlet and outlet pressure histories for use in BIFLO as boundary conditions. The pressures derived in this manner resulted in the calculation of the test section velocity history prior to boiling inception shown in Figure 10 of Reference 1.

The mass flow rates at the bundle inlet and outlet as calculated using a one-dimensional geometry in BIFLO are shown in Figure 1. The change in the slope of these curves which occurs ~6 s into the transient is a feature of the planned flow reduction in the experiment. The calculation indicates that boiling begins 11.70 s after initiation of the flow coastdown, followed by inlet flow reversal 0.547 s later (or 12.247 s after initiation of the flow coastdown).

The two-dimensional calculations indicated that intermittent boiling would begin in the corner adjacent to Pin 1 as early as 6.35 s into the flow coastdown; sustained boiling will not occur until 1.0 - 1.5 s later. Boiling will have developed across the entire bundle flow area by 10.793 s after initiation of the flow coastdown, followed by inlet flow reversal 0.549 s later (or 11.342 s after initiation of the flow coastdown). The mass flow rates at the bundle inlet and outlet calculated using a two-dimensional geometry in BIFLO are shown in Figure 2. The geometry used for this particular calculation did not isolate the corner region around Pin 1 as a single channel; cases which did isolate the region around Pin 1 exhibited mass flow rates having the same trends as those shown in Figure 2 but with different fine-structure fluctuations.

The calculations indicate that one- and two-dimensional analyses predict identical times for inlet flow reversal when time is measured relative to the time at which boiling has developed across the entire flow area of the bundle. The two-dimensional analysis, however, indicates that the absolute time (i.e. measured from the initiation of the flow coastdown) of inlet flow reversal is earlier than would be predicted by a one-dimensional analysis.

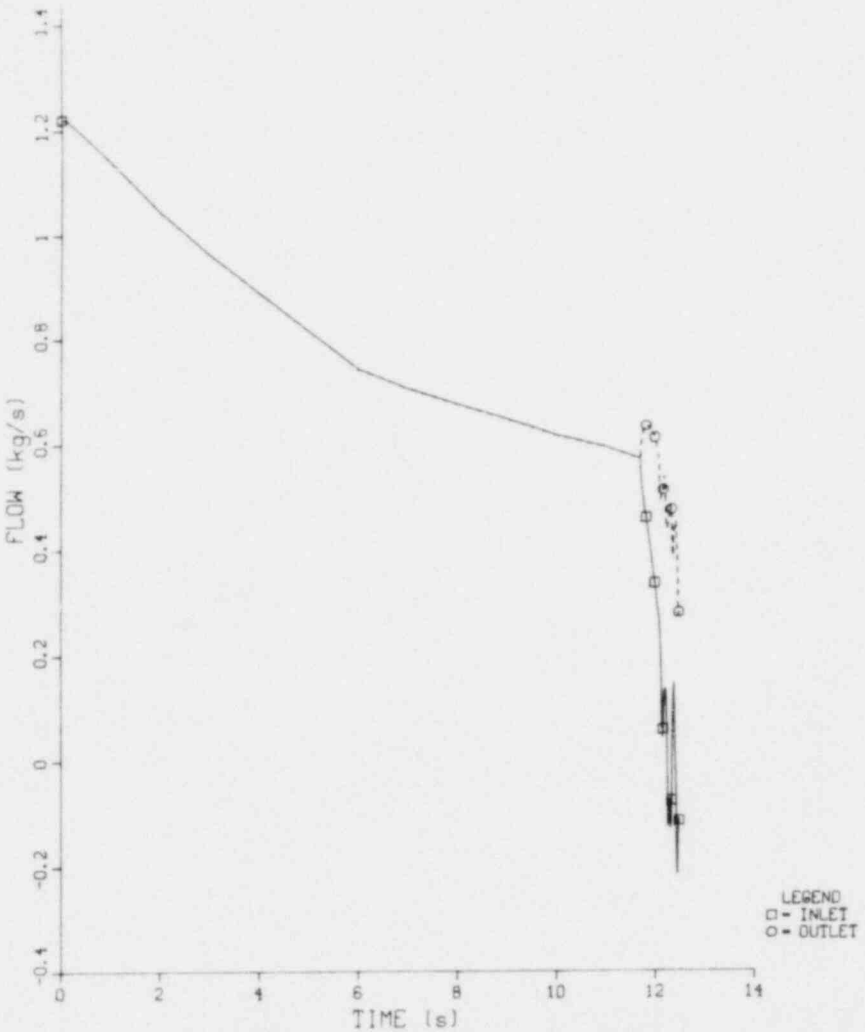

Fig. 1. Bundle Flow Rates Calculated Using a One-Dimensional Geometry in BIFLO for the 15-Pin OPERA Facility Experiment

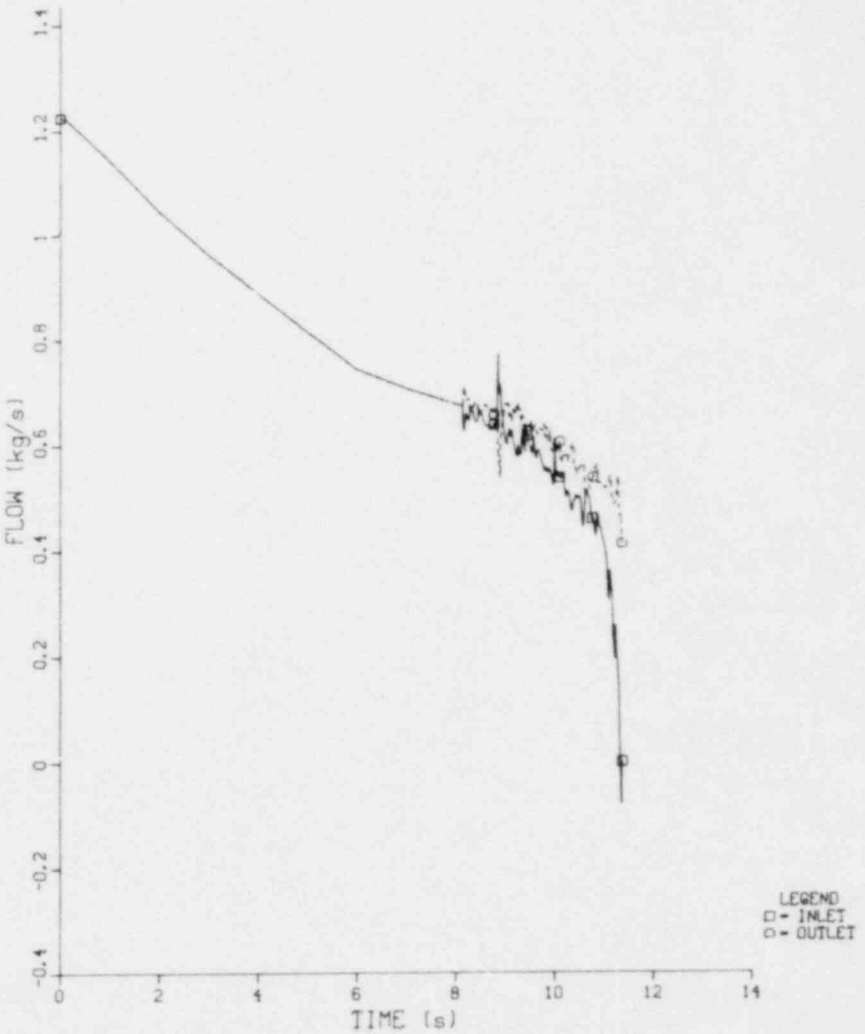

Fig. 2. Bundle Flow Rates Calculated Using a Two-Dimensional Geometry in BIFLO for the 15-Pin OPERA Facility Experiment

The trend of this result is in agreement with the theory[2] that early localized boiling diverts hot coolant from regions of high power-to-flow ratio to regions of low power-to-flow ratio and is an additional resistance to the total flow through the bundle. Since the overall bundle flow is governed by the boundary conditions of inlet and outlet pressure, the total bundle flow will decrease and the radially averaged coolant temperature will increase relative to those calculated with a one-dimensional model. The combination of lower flow rates and higher temperatures can result in earlier bulk boiling and more rapid progression of voiding than would be calculated using a one-dimensional model.

The magnitude of the difference in absolute timing of inlet flow reversal calculated by one- and two-dimensional analyses is somewhat surprising, although there is little published literature on this subject with which to compare. Most of the literature reporting comparisons of one- and two-dimensional calculations of boiling in fuel assemblies does not continue the analysis through the time of inlet flow reversal due to modeling inadequacies. Additionally, calculational models which use velocities rather than pressures as boundary conditions are not able to properly describe the effect which the early localized boiling has on the overall flow through the bundle. One clear comparison, however, was presented by Theofanous,[3] showing that one- and two-dimensional calculations of a loss-of-flow scenario in a 217-pin CRBR fuel assembly gave almost identical absolute timings for inlet flow reversal; inlet flow reversal in the two-dimensional analysis preceded the results from the one-dimensional analysis by only 0.03 s. A similar 217-pin bundle problem is being analyzed using BIFLO to see if the difference in results is due to the problem conditions (e.g. pressure histories and bundle power-to-flow characteristics) or due to modeling differences in the two codes. Reported results[4],[5] have more frequently shown that a one-dimensional calculation predicts voiding and inlet flow reversal too early when compared with data from tests in small bundles.

While awaiting release of the data from the 15-pin OPERA experiment, calculations are being performed for other (both smaller and larger) bundle geometries in order to see whether the pattern of results calculated for the 15-pin OPERA experiment is generic or specific. This work will also be useful when trying to extrapolate the results from the 15-pin OPERA experiment to the larger bundle sizes which the experiment hoped to simulate.

B. CRBR Initiating Phase Calculations with SAS3D/EPIC (P. A. Pizzica and H. H. Hummel)

1. Introduction

A number of preliminary calculations have been completed for the CRBR heterogeneous core for TOP and LOF transient conditions. For the TOP accident, three different points in the refueling cycle are being considered: BOC-1, EOC-3 and EOC-4. A fairly extensive study of EOC-3 TOP conditions has been completed but only very preliminary estimates have been made for the BOC-1 and EOC-4. For the LOF only EOC-4 has been considered so far.

2. TOP Calculations

To understand the significance of results obtained for the different points in the fuel cycle, the CRBR refueling scheme should be considered. At

the beginning of each odd-numbered fuel cycle, an entire fresh core loading consisting of 156 driver fuel assemblies and 82 inner blanket assemblies is installed. The first two cycles are anomalous in that the projected burnup is smaller than normal. However, the BOC-1 core configuration, consisting of all fresh fuel, is typical for the start of the odd-numbered cycles. Cycles 3 and 4 are typical of succeeding pairs of cycles. At the end of cycle 3, 6 inner blanket subassemblies are replaced with fresh driver fuel subassemblies to provide sufficient excess reactivity for cycle 4. These 6 subassemblies, operating at considerably higher power than the others in cycle 4, act as lead subassemblies in that they fail much earlier than the others.

In the BOC-1 core, a 10¢/s TOP transient has been calculated only as far as 13.25 sec. When a peak axial node fuel melt fraction of 0.58 is attained in the hottest SAS channel, which represents 24 out of the 156 subassemblies, 24 more subassemblies are only about 0.01 lower in peak fuel melt fraction. This means that almost a third of the driver subassemblies could fail at about the same time if fuel melt fraction can be correlated to failure time. Therefore, it is necessary to compute the case further and estimate the degree of coherency at failure conditions and the reactivity feedback of fuel and sodium motion resulting from pin failure. EPIC should provide significantly new information about the dynamics of fuel after failure since it currently has the best model available for fuel vapor driven ejection. Note that for fresh fuel the fuel motion characteristics are different from those for irradiated fuel because fuel moves under its own vapor pressure rather than under fission gas pressure.

For the EOC-4 core, a 10 ¢/s TOP has been calculated up to the point of pin failure in the lead 6 subassemblies. Even with a midplane failure assumed, these few subassemblies provide only a small amount of positive reactivity ($\sim$ 0.15 \$) in addition to 0.30 \$ net reactivity at failure before fuel sweepout brings the reactivity and power down. The amount of negative fuel sweepout reactivity is probably no more than 0.80 \$ to 1.0 \$, as estimated by the EPIC calculation. The calculation needs to be continued further to consider further pin failures which will result from further reactivity insertion. The next failures will occur only after some seconds of time delay, however. Therefore, the disposition of materials in the lead 6 subassemblies needs to be considered. These lead pins may heat up substantially if coolant flow is cut off because of fuel blockages in the channel. If this happens cladding could drain or move in some way and fuel could slump, leading to reactivity feedbacks which might affect further pin failures. Given the long time involved, considerable cladding and fuel motion could occur before subsequent pin failures. There is currently no way to treat this situation with SAS3D/EPIC; an external reactivity function based on separate estimates of material motion in these lead subassemblies may have to be used to continue the calculation.

A series of TOP calculations for the EOC-3 core was performed. Since no neutronics analysis has been done for the EOC-3 core which would have provided material worths and axial power distribution, these data were simply assumed to be the same as those for EOC-4. The same subassembly grouping was assumed as for EOC-4 and radial power factors were taken from the CRBR PSAR. The main difference between the EOC-3 and the EOC-4 cores, from the point of view of accident analysis, is that six core subassemblies have driver fuel in EOC-4 and have blanket pins in EOC-3. The result of this is that initial

failures are much more coherent for EOC-3 than for EOC-4, since a large fraction of the core has nearly the same power rating. With the assumed midplane failure, this was found to lead to an autocatalytic situation at high ramp rates.

Table I shows fuel melt fractions at the core midplane 50 msec before a 0.50 fuel melt fraction was attained in channel 10 during a 0.10 $/s TOP transient. It can be seen that 114 out of 156 driver subassemblies are within 3% of one another in peak fuel melt fraction and 66 out of 156 are within 1%. To the extent that pin failure can be correlated to fuel melt fraction, this situation indicates a very high potential for coherent pin failures across the core. It may be incorrect to attempt to correlate fuel melt fraction with pin failure, however.

TABLE I. EOC-3 Peak Fuel Melt Fraction for 10 ¢/s Ramp Rate

Channel No.	Number of Subassemblies	Fuel Type	Radial Power Factor	Fuel Melt[a] Fraction
1	7	Blanket	0.45	0.021
2	21	Driver	0.994	0.462
3	21	Blanket	0.468	0.142
4	9	Driver	0.998	0.464
5	36	Blanket	0.539	0.275
6	6	Blanket	0.493	0.189
7	12	Driver	1.084	0.487
8	12	Blanket	0.541	0.287
9	6	Driver	1.075	0.479
10	12	Driver	1.095	0.495
11	24	Driver	1.106	0.486
12	12	Driver	1.002	0.467
13	18	Driver	1.034	0.495
14	18	Driver	0.853	0.340
15	24	Driver	0.876	0.382

[a]At core midplane 50 msec before a 0.50 melt fraction was attained in channel 10.

A burst pressure pin failure criterion, which assumes the cladding to be stressed by fission gas pressure axially equilibrated along the length of the molten fuel, would predict the failure of cladding towards the upper end of the molten fuel cavity where the cladding is hotter and weaker. Such a criterion probably would have predicted failure at the point when the peak fuel melt fraction was in the range 0.40-0.50, depending upon assumptions used to calculate fission gas pressure and upon assumptions with respect to cladding strength. If, on the other hand, the mechanism of pin failure can be presumed to be differential fuel-cladding expansion, then it is possible that the location of the cladding breach and the subsequent release of molten fuel is near the midplane where the probability of such failure is highest. In order for such a release actually to occur, the fuel melt fraction must be sufficiently large and the pin gas pressure sufficiently high. Also, there must be a large enough break in the clad for molten fuel ejection to occur. In the following calculations, in order to assess the effects of such a midplane failure on the EOC-3 core, an 0.50 peak melt fraction was assumed to be necessary for the release of molten fuel.

Table II gives parametric assumptions and results of various cases calculated for TOP transients for the EOC-3 core. Cases 1 and 2 were run with 4.1 ¢/s driving reactivity ramp rates. Both cases had relatively high pin pressures at initial pin failure. Extension of the assumed 7 cm centerline rip was not allowed and the nominal EPIC FCI heat transfer coefficient[6] of $\frac{k_{fuel}}{r_p}$ was used. In both cases the pins in 18 subassemblies were assumed to fail coherently. The only differences between the two cases was that a different particle radius was assumed. In case 1, a 0.04 cm radius was used, implying a

TABLE II. EOC-3 TOP Calculations

Case Number	Ramp Rate ($/s)	Pin Pressure at Failure in Lead Pin (MPa)	Particle Radius Used in EPIC (cm)	FCI Heat Transfer Factor	Rip Extension Allowed	Net Reactivity at Pin Failure ($)	Total Number of Driver Subassemblies to Fail	Maximum P/P_o	Maximum Net Reactivity ($)
1	0.141	48	0.04	1.0	no	0.17	18	4	0.41
2	0.041	48	0.06	1.0	no	0.17	18	4	0.43
3	0.10	54	0.02	1.0	no	0.31	30	6	0.60
4	0.10	60	0.02	1.0	no	0.31	73	24	0.90
5	0.10	60	0.04	1.0	no	0.31	156	$>5.10^3$	>1.2
6	0.10	60	0.06	1.0	no	0.31	156	$>5.10^3$	>1.2
7	0.10	60	0.02	0.33	no	0.31	156	$>5.10^3$	>1.2
8	0.10	60	0.06	3.0	no	0.31	156	$>5.10^3$	>1.2
9	0.10	20	0.02	1.0	no	0.30	114	30	0.93
10	0.10	20	0.04	1.0	no	0.30	156	$>5.10^3$	>1.2
11	0.10	20	0.04	1.0	yes	0.30	156	$>5.10^3$	>1.2
12	0.50	38	0.04	1.0	no	0.61	156	$>5.10^3$	>1.2
13	0.50	15	0.02	1.0	no	0.62	156	$>5.10^3$	>1.2
14	0.50	15	0.04	1.0	no	0.62	156	$>5.10^3$	>1.2

20% of axial expansion feedback assumed effective in all TOP cases.

relatively inefficient FCI and fuel-sodium drag and case 2 assumed a very inefficient FCI and small drag. Even in case 2 with less fuel sweepout calculated because of the large particle radius, the reactivity did not rise sufficiently over the initial 0.17 $ level to raise the power level enough to produce further pin failures. In order for higher reactivity and power levels to have occurred, perhaps about 3 times as many pins would have had to fail within a 10-20 msec time period. This seems quite unlikely with the low ramp rate and power level (2.8 P/P_o at failure) which produces a quasi-steady state situation before pin failure.

Cases 3-11 were run with a 0.10 $/s ramp rate. The net reactivity level at first pin failure was ~0.30 $ and the power level was about 3.5 times nominal. In cases 3-8 the assumed initial pin pressures at failure were quite high; in cases 9-11 they were only about 1/3 as great. In case 3 the simultaneous failure of pins in 12 subassemblies was assumed and pins in 18 more subassemblies were assumed to fail ~10 msec later. No rip extension and nominal FCI heat transfer were assumed. A particle radius of 0.02 cm produced a quite efficient heat transfer and fuel-sodium drag which prevented high reactivity and power levels by promoting fuel sweepout. In case 4 the same assumptions were made as in case 3 except that pins in 30 subassemblies were assumed to fail simultaneously. This produced significantly higher reactivity and power levels and caused pins to fail in 42 more subassemblies but fairly efficient fuel sweepout due to the 0.02 cm particle radius prevented a worse situation. High reactivity and power levels were, however, attained when less efficient fuel sweepout was produced with larger particles in cases 5 and 6. Such high power levels were attained that very soon all driver pins were failed. In cases 7 and 8 the effect of the FCI heat transfer efficiency was tested. Case 7 was the same as case 4 except the FCI heat transfer coefficient was multiplied by a constant of 0.33. Case 8 was the same as case 6 except for the FCI factor of 3.0. Reducing the efficient heat transfer of case 4 resulted in high reactivity and power levels in case 7. But increasing the FCI heat transfer in case 8 did not prevent high reactivity and power levels which were also produced in case 6.

In cases 9-11, lower pin pressures were assumed at failure than in cases 3-8 and the simultaneous failure of pins in 30 subassemblies was assumed. Cases 9 and 10 were the same except for the size of the fuel particles which

again produced results similar to cases 4 and 5 with the smaller particle radius causing sufficient sweepout to prevent high power levels. In case 11, extension of the cladding rip was assumed to occur when a fuel melt fraction of 0.55 was produced at any axial cell. This rip extension did not prevent high power levels although the power level in case 11 was lower than in case 10. The reason for this result is that the rip extension has no effect on the calculation until more fuel melting occurs and this cannot happen as fast as necessary to prevent the reactivity from rising significantly above prompt critical because the power level even at prompt critical is only ~20 times nominal.

Cases 12-14 were run with a 0.50 $/s driving ramp. The initial net reactivity was ~0.62 $ and nominal power ~7.6. Nominal FCI heat transfer and no rip extension were assumed. The simultaneous failure of pins in 48 subassemblies, almost one-third of the driver pins, was assumed. In case 12, relatively high pin pressures were calculated at failure and a particle size of 0.04 cm was assumed. High power levels were attained. In case 13-14, lower pin pressures prevailed but two different particle radii of 0.02 and 0.04 were assumed. Because of the high initial reactivity level and the simultaneity of so many pin failures even the efficient sweepout of case 13 did not prevent high power levels.

It is apparent from this study that the most significant parameters involved are the simultaneity of pin failures, the efficiency of fuel sweepout and the initial reactivity level at pin failure, which is a function of the driving ramp rate.

For the case in which prompt criticality was attained the calculated power levels and maximum reactivity are not really meaningful because the only negative feedback in the calculation was from fuel sweepout. As the power and reactivity increase greatly, negative feedback from hydrodynamic disassembly will be present and must be calculated by a code other than SAS/EPIC. For a TOP such calculations in the past have given relatively small energy releases because of the rapid pressure buildup associated with the low void content of the core.

3. LOF Calculations

A number of cases were also calculated for a LOF transient to determine the potential for LOF-TOP pin failures in the EOC-4 core. In these calculations the fractional acceleration of gravity was varied parametrically. Fuel axial expansion feedback was assumed to either be 0.0 or 0.50 of the value corresponding to free thermal expansion. Clad motion was calculated using the KfK code CMOT.[7] Essentially no positive feedback was obtained from CMOT; instead small negative reactivity effects were obtained. It was found that the reason for this was that the calculated sodium vapor velocity was too small to levitate the molten clad for the assumed flooding velocity and friction factor. Because this velocity seems low for the calculated core pressure drop, the CMOT calculation is still under study. In any case large clad motion reactivity effects are not expected from CMOT, in contrast to those from the CLAZAS module[8] of SAS3D.

The following cases were run with full gravity slumping and no fission gas or steel or sodium vapor driven fuel dispersal assumed for all

slumping pins (i.e. 108 out of 162 subassemblies). First of all two cases were run, one with no axial expansion reactivity feedback assumed and one with 50% of the axial expansion feedback corresponding to free thermal expansion. Although cladding temperatures were somewhat hotter in the case with axial expansion feedback, there was roughly the same amount of potential for LOF-TOP failures in each case, with the pins of 54 subassemblies calculated to undergo such failure in both cases. Two options were used for LOF-TOP failures in the case with axial expansion feedback. A 0.50 fuel melt fraction failure criterion with a 15 cm cladding breach assumed not to extend was used in the first case and the 0.50 melt fraction with an intial 55 cm cladding breach was used in the second case. With the short rip, the nominal reactor power went to $\sim 2.10^4$. Even with the long breach the nominal power went to $\sim 5.10^3$. Without such LOF-TOP failures, the reactor power would have reached only several hundred times nominal. If LOF-TOP pin failures are delayed in these cases until their peak fuel melt fraction is higher than about 0.80, then there is enough fuel dispersion driven by fuel vapor to shut down the reactor and preclude LOF-TOP failure.

In a case run with the same assumptions as above except with 0.1 g applied to slumping fuel, no LOF-TOP pin failures were calculated although the reactor power reached several hundred times nominal. However it was apparent from this run that if slumping ramp rates had been only slightly higher, LOF-TOP failures might have become possible.

II. THREE-DIMENSIONAL CODE DEVELOPMENT FOR CORE THERMAL-HYDRAULIC ANALYSIS OF LMFBR ACCIDENTS UNDER NATURAL CONVECTION CONDITIONS

A2045

A. Introduction

The objective of this program is to develop computer programs (COMMIX and BODYFIT) which can be used for either single-phase or two-phase thermal-hydraulic analysis of reactor components under normal and off-normal operating conditions, especially under natural circulation. The governing equations of conservation of mass, momentum, and energy are solved as a boundary value problem in space and an initial value problem in time.

COMMIX is a three-dimensional, transient, compressible flow computer code for reactor thermal-hydraulic analysis. It is a component code and uses a porous medium formulation to permit analysis of a reactor component/multicomponent system such as fuel assembly/assemblies, plenum, piping system, etc., or any combination of these components. The concept of volume porosity, surface permeability, and distributed resistance and heat source (or sink) is employed in the COMMIX code for quasi-continuum (or rod-bundle) thermal-hydraulic analysis. It provides a greater range of applicability and an improved accuracy than subchannel analysis. By setting volume porosity and surface permeability equal to unity, and resistance equal to zero, the COMMIX code can equally handle continuum problems (reactor inlet or outlet plenum, etc.).

BODYFIT is a three-dimensional, transient, compressible flow computer code for reactor rod bundle thermal-hydraulic analysis. This is also a component code, and it uses a boundary-fitted coordinate transformation. The complex rod bundle geometry is transformed into either rectangular or cylindrical coordinates with uniform mesh. Thus, the physical boundaries, including each rod, coincide with computational grids. This allows the Navier-Stokes equations, together with the boundary conditions, to be represented accurately in the finite-difference formulation. Thus, the region in the immediate vicinity of solid surfaces, which is generally dominant in determining the character of the flow, can be accurately resolved.

B. COMMIX-1A, Single-Phase Code Development (W. L. Baumann, H. M. Domanus, J. R. Hull, R. C. Schmitt, W. T. Sha, J. E. Sullivan, and S. P. Vanka)

B.1 Development Work

During this quarter, the following improvements and modifications were implemented in the code:

- A new operating procedure for obtaining load modules was developed to take advantage of the dynamic storage capability of version 7.0. While previous versions required the user to make changes to several variables directly in the COMMON blocks, the new procedure will require the specification of only one space allocation parameter. Moreover, if this parameter is not known, it can be automatically

determined by running the input data through any existing load module.

- Several subroutines have been modified to permit optional creation of an automatic double-precision load module.
- The arguments of all property-calling subroutines were modified to provide flexibility in using different property packages.
- Modifications were implemented in thermal structure model to permit, for each thermal structure, a different transient function for volumetric heat source.
- Changes in plottape and related changes in graphic packages were made to permit writing of all variables related to thermal structure.
- An option has been provided in graphic package to permit automatic scaling of vectors and isotherm plots.
- Improvements and updatings are performed in the graphic package capability of plotting dependent variables as functions of time.
- The thermal interaction term in the thermal structure model has been reformulated in an implicit form. This formulation has relieved occurrence of occasional instability.
- An option has been implemented permitting printing of results at prescribed values of time or at prescribed values of time step. This option is now being tested.
- Efforts are continuing to detect any bugs, if they exist and correct them.
- Efforts have begun to document and release the code.

B.2 Validation of COMMIX-1A for Preparation of CRBR Licensing

FFTF Simulation

Steady-State Simulation

The three-dimensional steady-state in-vessel thermal hydraulics of the Fast Flux Test Facility is analyzed. The important input data for FFTF simulation are presented in Appendix A. The finite-difference grid is shown in Figs. 3 and 4.

The coolant flow path has been sketched in Fig. 5. As expected, the output from the COMMIX code displays a similar flow path. The inlet flow enters the inlet plenum, flows upwards to the core basket and the shield, and subsequently enters the outlet plenum. There are three outlets located 120° apart in the outlet plenum.

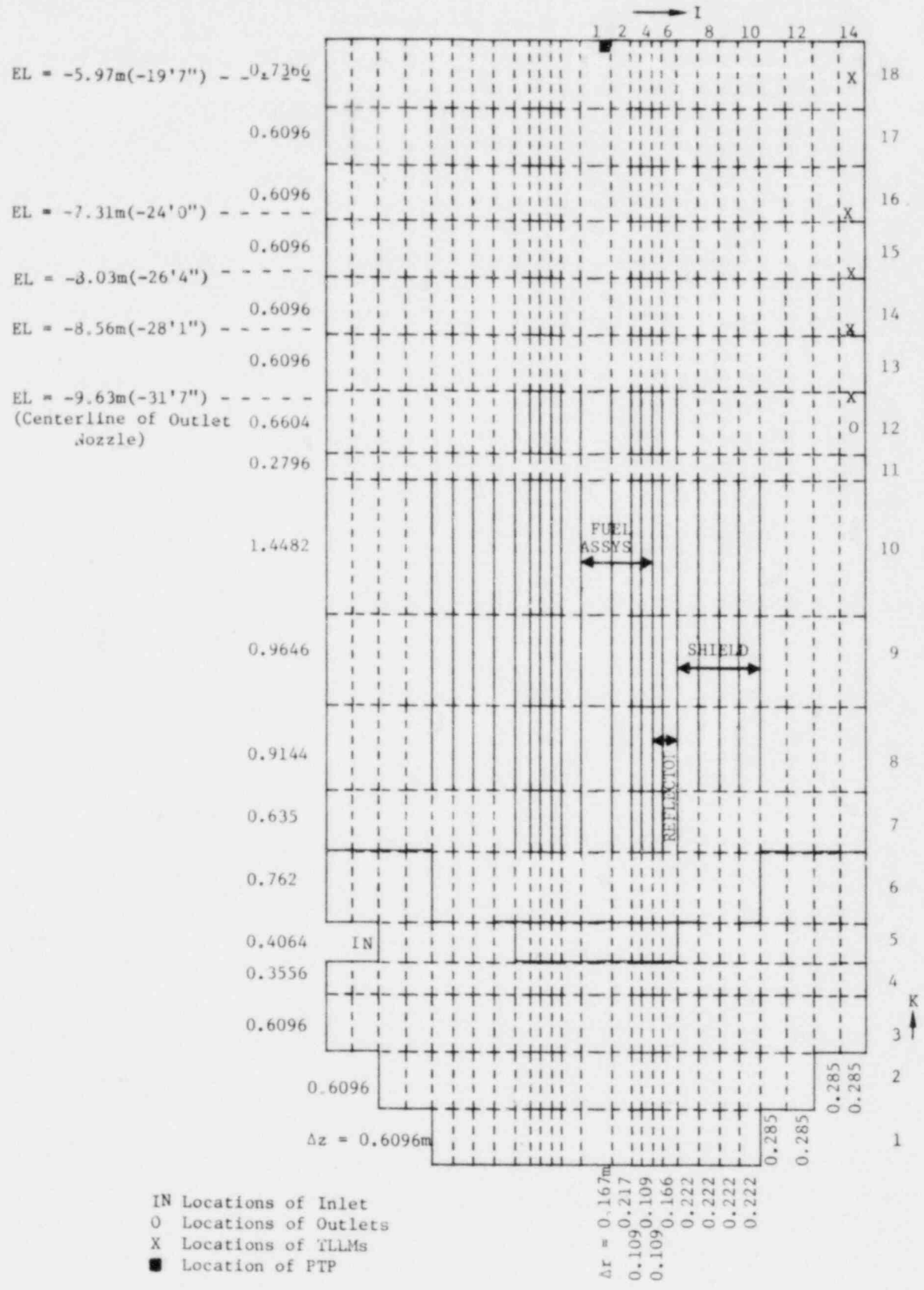

Fig. 3. Finite-Difference Grid in R-Z Plane

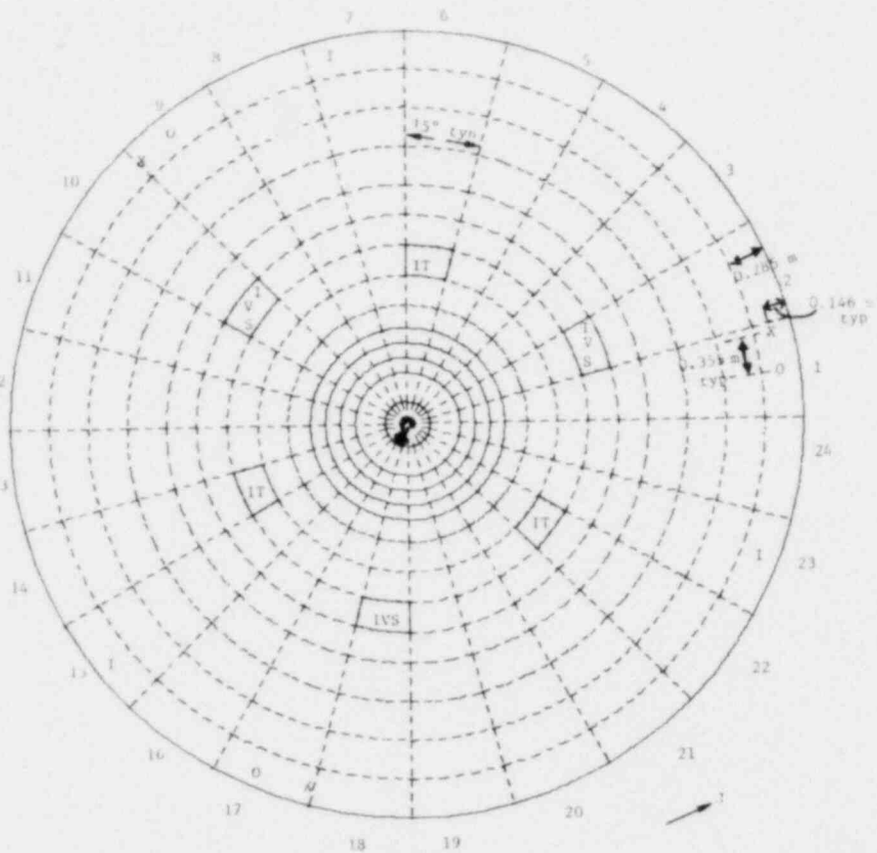

Fig. 4. Finite-Difference Grid in R-θ Plane

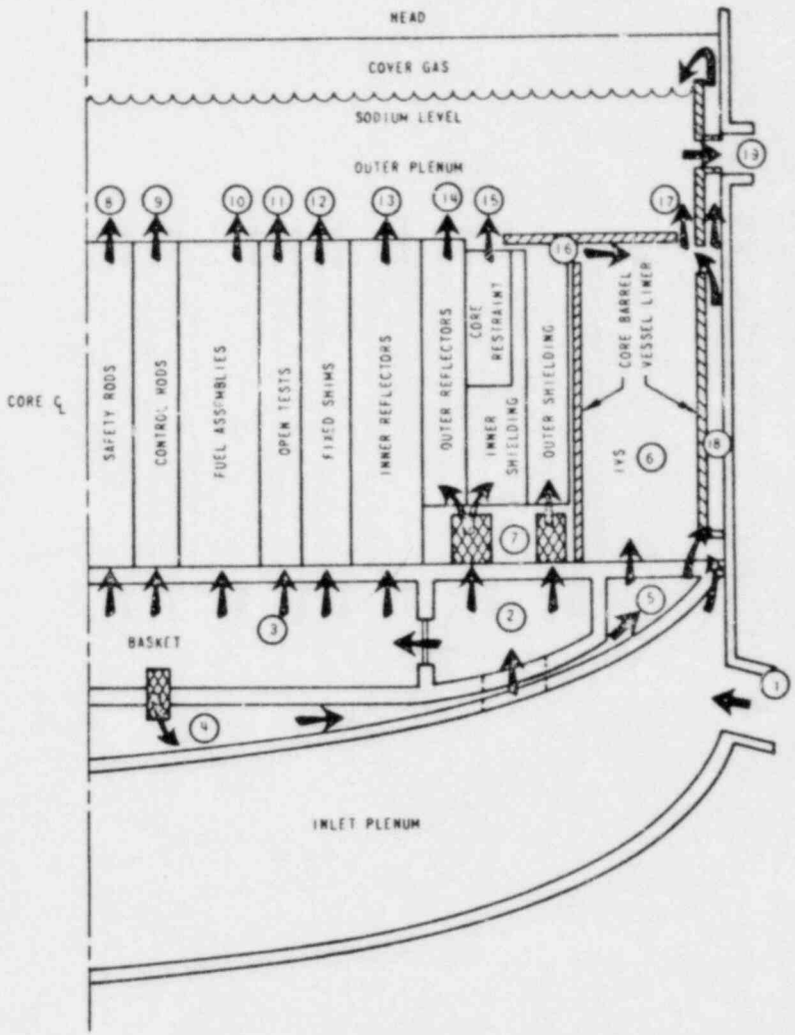

Fig. 5. Reactor Vessel Flow Distribution

The output from the calculations is a detailed description of the velocities and temperatures at 5901 nodes in the reactor vessel. Since it is difficult to present all this information concisely, we have plotted the flow patterns in various planes (axial and azimuthal) to illustrate the flow distribution. These are shown in Figs. 6-8. The comparison of calculations with experiments at steady state have been made of flow rates and temperatures at selected locations. These are tabulated in Tables 3 and 4. It is seen that, but for minor differences, the agreement is satisfactory between experiments and calculations. The temperature contours are shown in Fig. 9 for planes J = 4 and 16. It can be seen that there is appreciable three-dimensionality in the flow and temperature, notably because of differences in power output and the locations of outlet nozzles. There is also an effect due to the presence of the internal obstacles such as the Instrument Tree Stem and the In-Vessel Handling Machine Stem.

Discussion of Results

From the results presented in earlier figures, the following phenomena are worth observation: First, there is significant three-dimensionality in the flow, especially above the core. There are secondary vortex-type flows in the lower plenum. Above the core, the flow exiting the core fans out at the top, and as seen in Fig. 8 (K = 18), flows radially outwards to the outlet. In the r-z planes, a vortex flow is set up with downward flow near the outer wall, and upward flow at the core.

The temperature contours show temperature stratification below the level of the outlet nozzles. The low temperatures reflect the cold flow exiting the reflectors, liner, and the shield. The hot fluid represents the core exit flow. Stratification occurs near (or at) the outlet, and as it can be seen in the isotherms, there is a significant temperature gradient at and near the outlet nozzles.

The tabulated temperatures show good agreement between calculated and experimental data, except for the temperature measured by the PTP (Proximity Test Plug). The discrepancy may be due to inadequate mixing of the hot inner fluid with the colder fluid from adjacent (row 3) assemblies. The present model employs very coarse mesh and also does not exactly model the flow paths in the instrument-tree tubes. The calculated results can be improved by rigorously modeling the geometry just above the core with finer computational mesh.

Transient Simulation

The FFTF simulations have been performed for the case of transient flow and temperature fields following a reactor scram from 100% power. The power function from Brookhaven was used. Two sets of simulations were performed. In the first set, the FFTF geometry was modeled as two-dimensional, and in the second case, a 120° sector of the geometry was simulated. Two-sided thermal structures were used in the core and reflector regions. Two different transient functions were used to input exactly the power decay function in the reflector zone. The calculations have been carried out up to a real time of 79 secs. The calculated temperatures of FOTA, TLLMs, and PTP agree satisfactorily with the data. A report describing the steady state and transient calculations is under preparation.

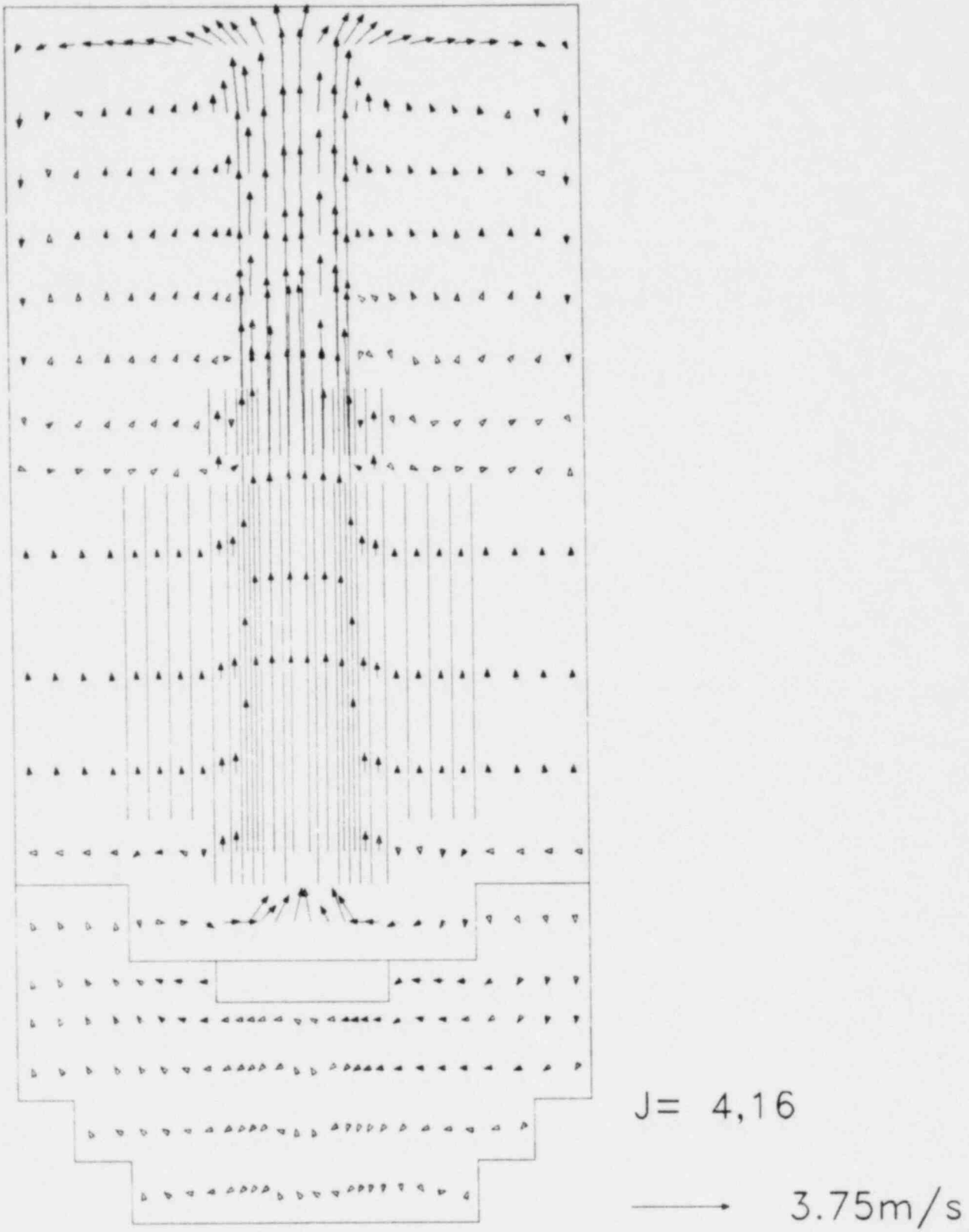

Fig. 6. Velocity Vectors in R-Z Plane

Fig. 7. Velocity Vectors in R-θ Plane

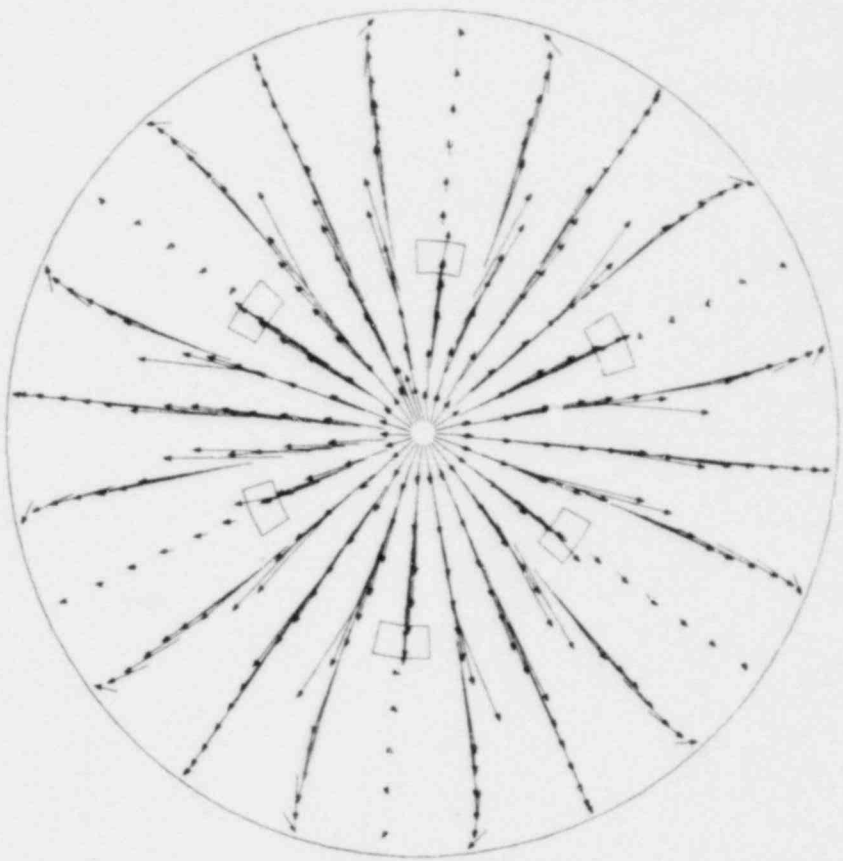

Fig. 8. Velocity Vectors in R-θ Plane

Table 3. COMPARISON OF STEADY-STATE FUEL-ASSEMBLY OUTLET TEMPERATURES AND FLOWS[†]

CELL (I,J) (r,θ)	CALCULATED FLOW (gpm)	MEASURED FLOW (gpm)	CALCULATED TEMPERATURE (°C)	MEASURED TEMPERATURE (°C)
1,1*	164.1	166.7	541.9	547.9
1,2	158.1	155.4	550.1	548.3
1,10	157.8	164.2	544.7	545.4
2,7	436.9	437.5	515.7	526.8
2,8	436.9	425.0	515.3	527.3
2,10	535.9	542.5	514.2	514.4
2,12	536.0	537.2	514.6	512.3
3,2	265.2	256.2	511.2	512.7
3,5	265.1	256.2	510.4	514.9
3,9	529.5	522.5	526.6	531.0
3,12	264.4	263.7	502.7	504.9
3.15	528.3	520.0	525.0	517.4
3.18	265.1	270.0	510.5	504.7
3,24	529.7	520.0	525.7	528.2
4,1	522.9	547.5	530.6	522.9
4,3	521.4	540.0	521.4	512.6
4,7*	531.1	526.2	521.8	520.0
4,12	518.8	520	507.7	500.0
4,14	314.8	307.5	522.8	504.6
4,22	312.7	312.5	505.4	499.5

*FOTA

[†]The flows and temperatures are measured in instrument-tree guide tubes (approximately 0.3 m long) located above the assemblies.

Table 4. COMPARISON OF TEMPERATURES IN OUTLET PLENUM[†]

LOCATION	CALCULATED TEMPERATURE (°C)	MEASURED TEMPERATURE (°C)
TLLM (-19'.7")	510.8	507.4
TLLM (-24'.0")	511.1	511.27
TLLM (-26'.4")	511.5	509.3
TLLM (-28'.1")	511.8	514.77
TLLM (-30'.7")	507.5	509.3
PTP	542.4	527.0
TOTAL ΔT THROUGH VESSEL	143.22	143.33
INSTRUMENT TREE STALK TEMPERATURES	436.2 (J = 6)	440.1
	436.7 (J = 14)	435.0
	436.8 (J = 22)	437.7

[†]See Figs. 3 and 4 for locations of TLLMs and PTP in R-Z and R-θ planes.

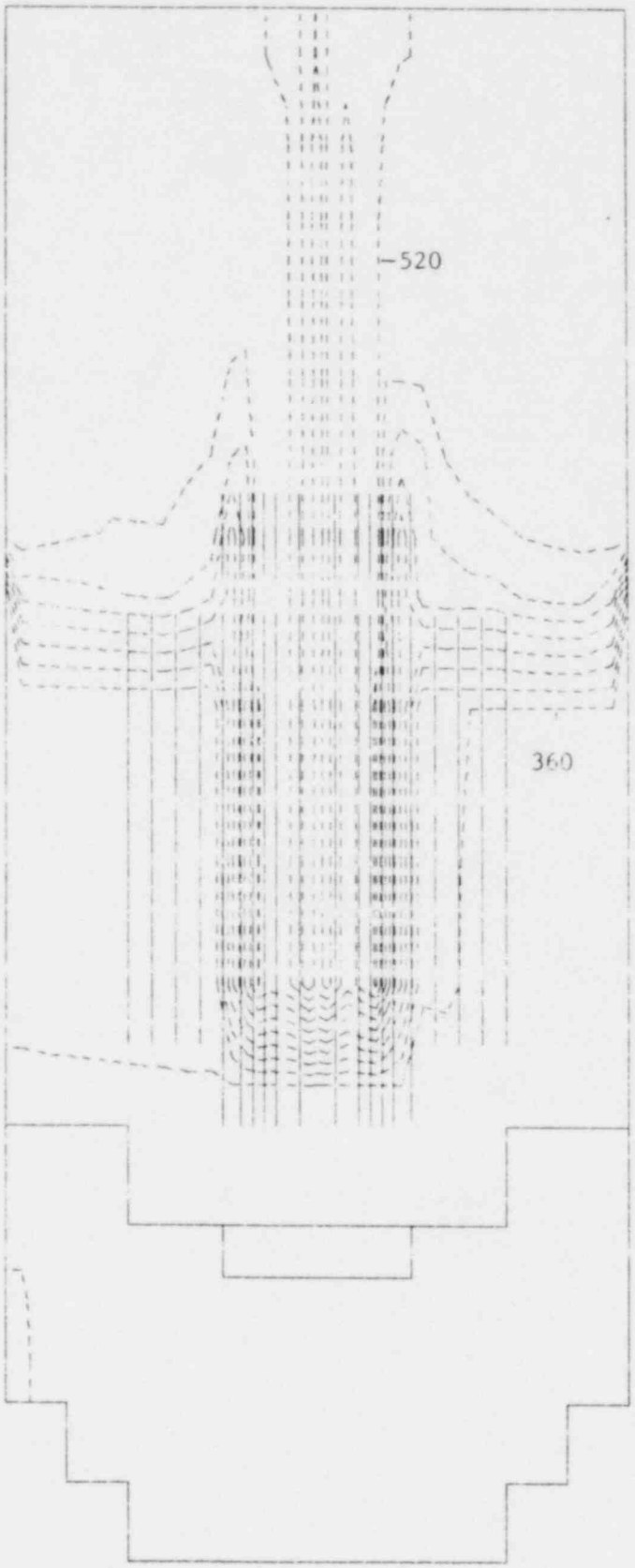

Fig. 9. Temperature Isotherms for Planes J = 4 (left) and J = 16 (right)

CRBR Primary Vessel

Work has been initiated to simulate thermal-hydraulic conditions in the CRBR primary vessel. Geometrical features based on available information from PSAR are modeled. The input data is now being tested. In the meantime, efforts are being made to obtain latest drawings of the CRBR vessel. These drawings will provide detailed information and dimensions of internal strucures which are required for proper modeling.

Simulation of EBR-II Pool Reactor Test

Analysis of the EBR-II Pool Reactor Transient Test #10 (Natural Circulation) has been performed. The case being investigated is the low-power, high-flow case. To save computer time and storage cost, a 1/16th azimuthal section of the geometry was modeled. A total of 32 thermal structures was modeled to simulate heat transfer from and heat capacity of the fuel pins and shrouds. The implicit formulation of COMMIX-1A was used for both steady and transient analysis. The full transient (200 s) simulation has been performed. The numerical results are in agreement with experimental data. The final report is under preparation.

C. COMMIX-2, Two-Phase Code Development (H. M. Domanus, C. C. Miao, W. T. Sha, and V. L. Shah)

During this quarter, most efforts were spent in determining the effects of various relaxation parameters. It was observed that implicit under-relaxation (under-relaxation of coefficients) of the pressure equation is sometimes unstable. The code is therefore modified and explicit under-relaxation (under-relaxation at the end of the solution of a set of linear algebraic equations) of the pressure equation is provided. It was further observed that when boiling starts, the under-relaxation of density is important to stabilize the solution.

In order to ensure that all modifications in COMMIX-2 have not brought any errors, the German seven-pin transient test was resimulated. The resimulation was extended to a transient period of 10.24 seconds. Efforts are now being made to continue simulation of the German seven-pin test to a longer transient period time.

D. BODYFIT Code Development (B. C-J. Chen and W. T. Sha)

During this quarter, the new pressure-correction scheme was implemented by using finite-differenced momentum equation and local geometric coefficients. This new scheme speeds up the rate of calculational convergence tremendously as can be seen in Figs. 10-12. A sample case was set up to compare the new scheme and the previous scheme. A 3x3 rod bundle with dimensions typical of a commercial boiling water reactor (BWR) fuel assembly was used for the sample case. All inlet and operating conditions are typical BWR conditions. Figures 10-12 show the change of axial velocities, enthalpies, and mass residues respectively, as a function of iteration numbers. As clearly shown in the figures, the new scheme gave much faster rate of convergence than the previous scheme did. In the coming month, we will use this new scheme to improve the calculation of flows in a 90°-bend elbow.

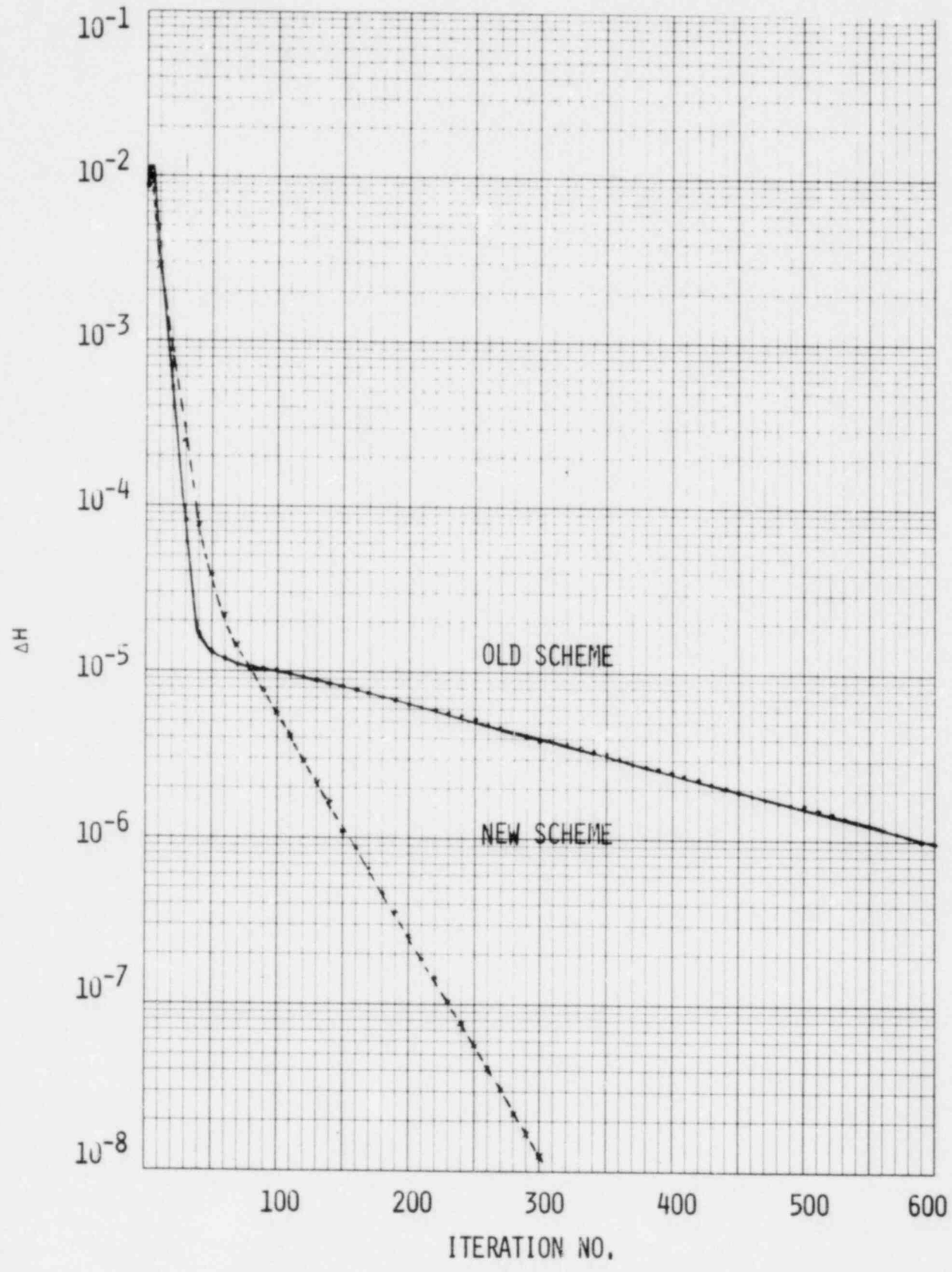

Fig. 10. Change of Enthalpy as Function of Iteration Number

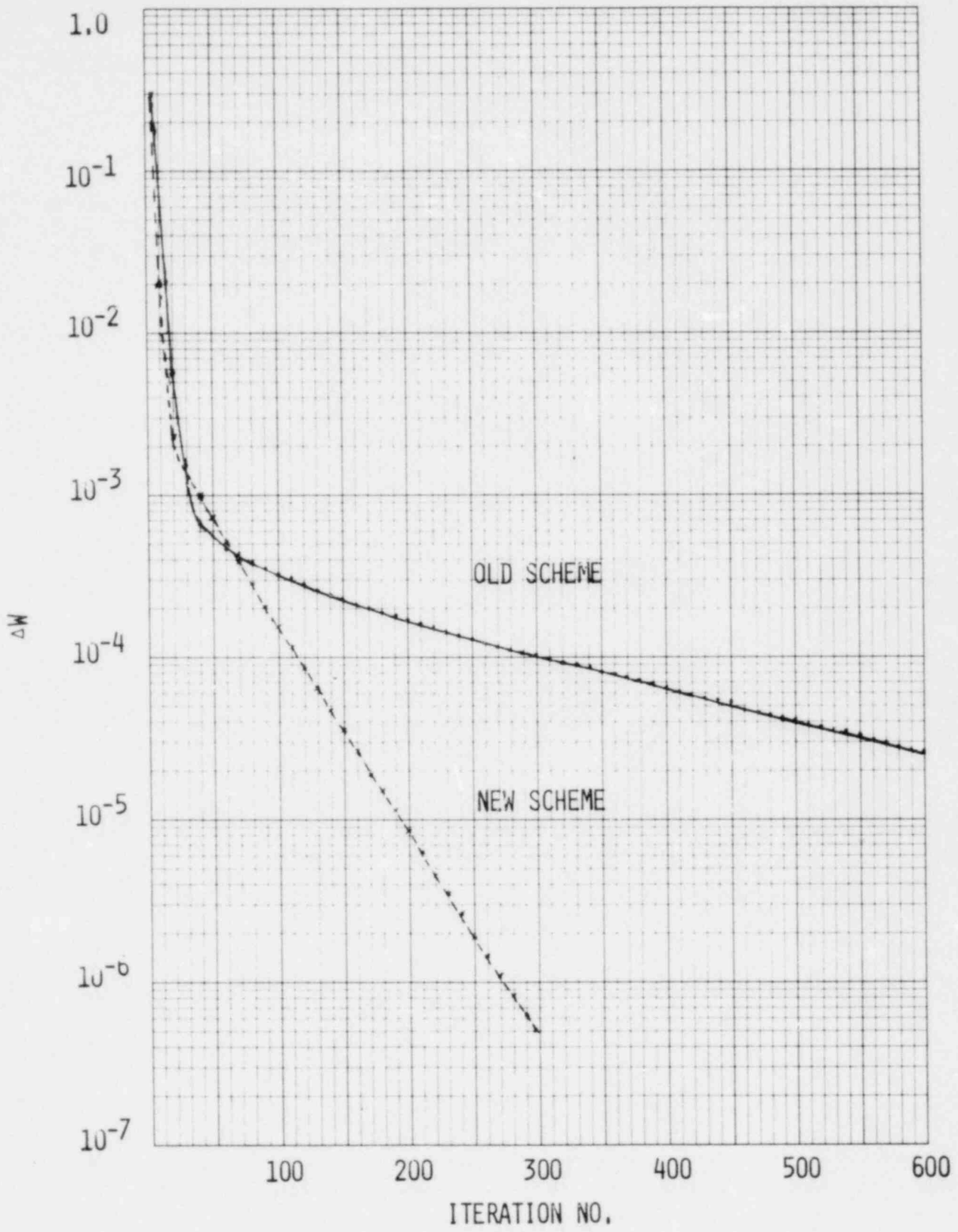

Fig. 11. Change of Velocity as Function of Iteration Number

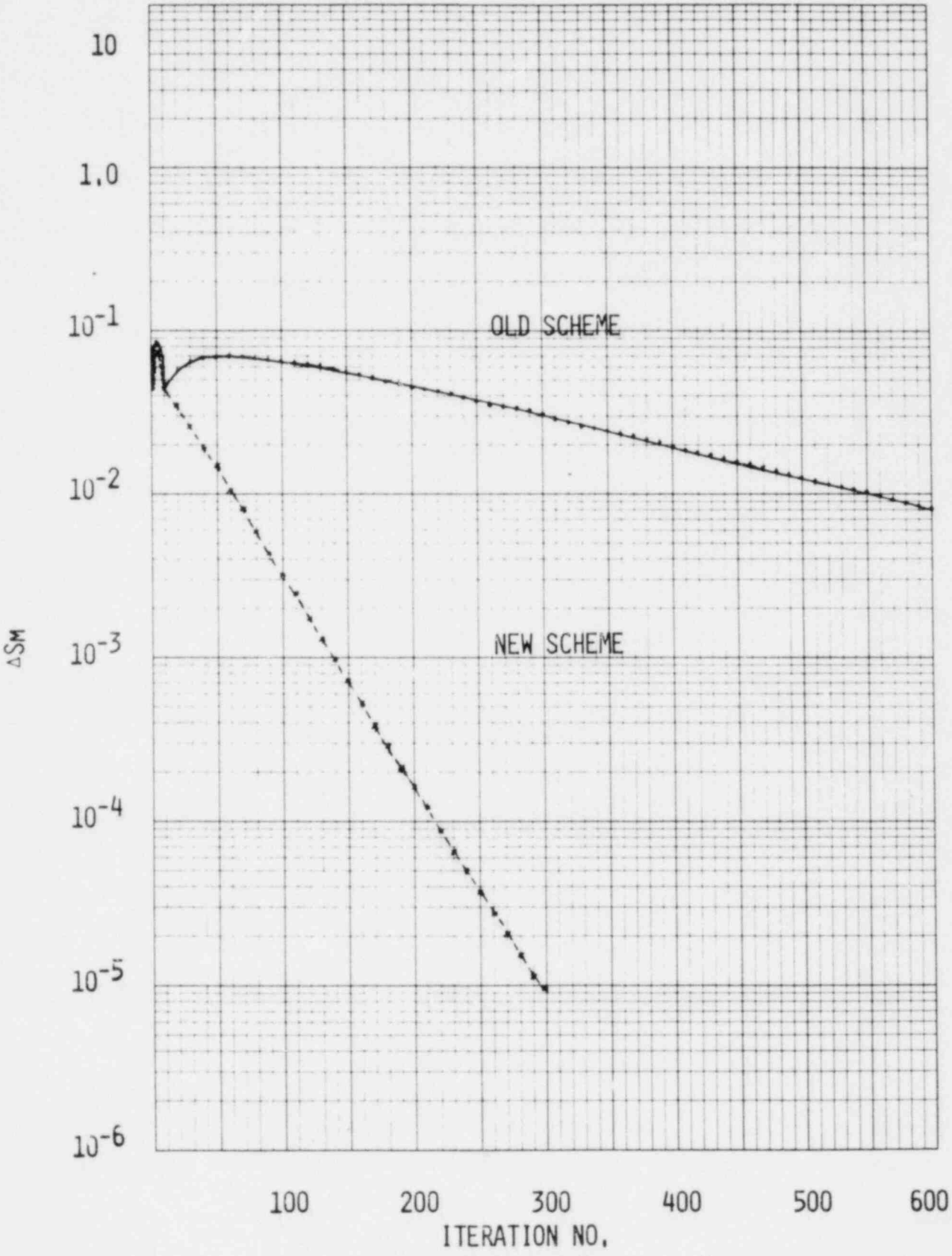

Fig. 12. Change of Mass Residue as Function of Iteration Number

REFERENCES

1. T. J. Scale, "Pretest Information Package for OPERA 15-Pin Experiment," ANL/RAS 81-32, Argonne National Laboratory (1981).

2. Hans K. Fauske, "Some Comments on Sodium Behavior (Boiling) in LMFBR Wire-Wrapped Subassemblies," Trans. Am. Nucl. Soc., 27, 570-571 (1977).

3. T. G. Theofanous, "Multiphase Transients with Coolant and Core Materials in LMFBR Core Disruptive Accident Energetics Evaluation," NUREG/CR-0224, 148-149 (1978).

4. W. W. Marr and I. T. Hwang, "An Approach for Treating Two-Dimensional Coolant Boiling in an LMFBR Fuel Subassembly," Trans. Am. Nucl. Soc., 27, 569-570 (1977).

5. I. T. Hwang et al., "Sodium Voiding Dynamics and Cladding Motion in a 37-Pin Fuel Assembly During a LOF Transient," Trans. Am. Nucl. Soc., 28, 443-445 (1978).

6. P. A. Pizzica et al., "A User's Guide to EPIC, A Computer Program to Calculate the Motion of Fuel and Coolant Subsequent to Pin Failure in an LMFBR," NUREG/CP-1504, ANL-80-47 (October 1979).

7. G. Angerer and D. Woll, "Simulation of Cladding Relocation in the TREAT Experiment R5 with the CMOT Code," Specialists' Workshop on Prediction Analysis of Material Dynamics in LMFBR Safety Experiments, March 13-15, 1979, Los Alamos Scientific Laboratory, LA-7938C, p. 185.

8. W. R. Bohl and T. J. Heames, "CLAZAS: The SAS3A Clad Motion Model," ANL/RAS 74-15, Argonne National Laboratory (August 1974).

APPENDIX A

IMPORTANT INPUT DATA FOR FFTF SIMULATION

A.1 Dimensions

The dimensions were obtained either from the FSAR or from the design drawings obtained from HEDL. It is not possible and also not relevant to list all design dimensions that were used to simulate the geometry. However, we shall mention below the most important dimensions, which will enable the reader to obtain a picture of the facility. A listing of the input description to COMMIX-1A is also enclosed at the end of this appendix.

Vessel Radius	2.911 m
Vessel Height (considered for present calculations)	12.04 m
Inlet-pipe diameter	0.4064 m (16 in.)
Outlet-pipe diameter	0.7112 m (28 in.)
Number of pins per assembly	217
Pin diameter	0.00584 m (0.230 in.)
Number of assemblies (including nonfueled)	91

A.2 Flow Rates and Temperatures

Total inlet flow	2203 kg/s (40,330 gpm)
Inlet temperature	360°C
Outlet temperature	503.3°C

A.3 Boundary Conditions

Inlet	Prescribed velocity and temperature
Outlet	Zero-gradients of velocity and temperature
Walls	Adiabatic

A.4 Finite-Difference Grid

The finite-difference grid consisted of 5901 cells, with 18 axial partitions, 15 radial partitions, and 24 azimuthal partitions. The finite-difference grid is sketched in Fig. 6.

Distribution for NUREG/CR-2774 Vol. I (ANL-82-24 Vol. I)

Internal:

E. S. Beckjord
C. E. Till
F. S. Onesto
R. Avery
P. B. Abramson
I. Bornstein/
A. B. Klickman
C. E. Dickerman
F. E. Dunn
D. Ferguson/L. Baker
S. H. Fistedis
P. L. Garner
E. Gelbard
H. Henryson
H. H. Hummel (3)
I. T. Hwang
Kalimullah
M. F. Kennedy
D. H. Lennox
L. G. LeSage
D. J. Malloy
P. Pizzica
F. G. Prohammer
D. Rose/A. J. Goldman/
J. F. Marchaterre
R. Sevy
J. J. Sienicki
W. J. Sturm
B. J. Toppel
J. B. van Erp
D. Weber
H. Wider
H. M. Domanus
V. L. Shah
B. C-J. Chen
W. T. Sha
P. I. Amundson/
S. G. Carpenter
M. J. Lineberry
D. H. Shaftman
A. Travelli
ANL Contract File
ANL Patent Dept.
ANL Libraries (2)
TIS Files (3)

External:

USNRC, Washington, for distribution per R7 (295)
DOE-TIC, Oak Ridge (2)
Manager, Chicago Operations Office, DOE
President, Argonne Universities Association, Argonne, Ill.
Applied Physics Division Review Committee:
P. W. Dickson, Jr., Clinch River Breeder Reactor Project, Oak Ridge, Tenn. 37830
K. D. Lathrop, Los Alamos Scientific Lab., P. O. Box 1663, Los Alamos, N. M. 87545
D. A. Meneley, Ontario Hydro, 700 University Ave., Toronto, Canada M5G 1X6
J. E. Meyer, Massachusetts Inst. Technology, Cambridge, Mass. 02139.
R. Sher, Stanford U., Stanford, Calif. 94305
C. Spight, AMAF Industries, Inc., P. O. Box 1100, Columbia, Md. 21044
D. B. Wehmeyer, The Detroit Edison Co., 2000 Second Ave., Detroit, Mich. 48226
Components Technology Division Review Committee:
A. A. Bishop, U. Pittsburgh, Pittsburgh, Pa. 15261
F. W. Buckman, Consumers Power Co., 1945 Parnell Rd., Jackson, Mich. 49201
R. Cohen, Purdue U., West Lafayette, Ind. 47907
R. A. Greenkorn, Purdue U., West Lafayette, Ind. 47907
W. M. Jacobi, Westinghouse Electric Corp., Nuclear Fuel Div., Pittsburgh, Pa. 15230
E. E. Ungar, Bolt Beranek and Newman Inc., 50 Moulton St., Cambridge, Mass. 02138
J. Weisman, U. Cincinnati, Cincinnati, O. 45221
C. Erdman, Texas A&M U., College Station, Tex. 77843
K. O. Ott, Purdue U., West Lafayette, Ind. 47907
R. Lancet, Atomics International, P. O. Box 309, Canoga Park, Calif. 91304